Chemical Engineering Journal 502 (2024) 157842

Contents lists available at ScienceDirect

Chemical Engineering Journal

journal homepage: www.elsevier.com/locate/cej

Minimizing solvated water via synergistic effect of salt anion and cosolvent enables stable Zn metal anodes in low-cost acetate electrolyte

Huifang Fei [a,b], Fuhua Yang [a,b,*], Jodie A. Yuwono [d], Maider Zarrabeitia [a,b], Stefano Passerini [a,b,c], Alberto Varzi [a,b,**]

[a] Helmholtz Institute Ulm (HIU), Helmholtzstrasse 11, D-89081 Ulm, Germany
[b] Karlsruhe Institute of Technology (KIT), P.O. Box 3640, D-76021 Karlsruhe, Germany
[c] Austrian Institute of Technology (AIT), Center for Transport Technologies, Giefinggasse 2, 1210 Wien, Austria
[d] School of Chemical Engineering, The University of Adelaide, Adelaide, South Australia, 5005 Australia

ARTICLE INFO

Keywords:
Zinc metal anode
Acetate
Co-solvent
Trimethyl phosphate

ABSTRACT

Aqueous zinc metal batteries (ZMBs) have attracted increasing attention in the past decades owing to their potentially low cost and non-flammability. However, the poor Coulombic efficiency (CE) and short lifespan caused by side reactions (e.g., H_2 evolution) and dendrite growth limit the practical applications of ZMBs. Given that H_2 evolution is primarily originated from solvated water, here, a low-cost acetate-based electrolyte constituted by 1 m $ZnAc_2$ and 5 m KAc in an 80:20 water:trimethyl phosphate (TMP) (v/v) mixture is proposed to minimize solvated water and boost the electrochemical performance of aqueous ZMBs without compromising intrinsic advantages of the aqueous electrolyte. The relatively high abundance of Ac^- enables preferential coordination with Zn^{2+}, meanwhile, the addition of TMP not only further replaces water molecules in the inner solvation shell, but also significantly interrupts the H-bond network of water. Improved electrochemical performance are demonstrated in Zn||Zn and Zn||Cu half-cells and Zn||I_2 full cells.

1. Introduction

Lithium-ion batteries (LIBs) are largely employed in portable electronic devices and electrical vehicles, due to their relatively high energy density [1,2]. However, the organic electrolyte employed in LIBs not only poses safety hazards due to its flammability, but also makes LIBs relatively expensive [3,4]. In this regard, aqueous batteries are considered as a promising alternative to LIBs for grid-scale energy storage systems because of their intrinsic advantages of low production cost, high safety and environmental friendliness. Among the possible aqueous battery chemistries, e.g., Na-, K- and Mg- based batteries, zinc metal batteries (ZMBs), allow the direct use of zinc metal as anode. The Zn metal anode features high specific capacity (820 mAh/g) and low redox potential close to the cathodic limit of aqueous electrolytes (−0.763 V vs. SHE), resulting in relatively high energy density of ZMBs [5]. The major issue impeding the practical application of rechargeable ZMBs is the poor reversibility arising from the H_2 evolution and other associated parasitic reactions occurring at the zinc metal anode [6,7]. As a result, battery failure occurs due to electrolyte and/or electrode depletion.

In a typical zinc aqueous electrolyte, Zn^{2+} is solvated by six water molecules to form a hydrated zinc ion, $[Zn(H_2O)_6]^{2+}$. According to the current understanding, H_2 evolution is primarily originating from solvated water rather than the free-state water molecules [8]. Therefore, efforts have been devoted to minimizing solvated water molecules in the aqueous electrolyte to suppress the corrosion reaction and the associated H_2 evolution. Organic co-solvent represents one of the most promising strategies to minimize H_2 evolution, expand the electrochemical stability window, and in some cases, regulate Zn deposition behavior. These organic compounds are capable of replacing water molecules in the inner solvation shell due to their ability to coordinate Zn^{2+} more strongly than water. However, in most cases, such co-solvents (e.g., N,N-dimethylformamide [9] and diethyl carbonate [10]) are flammable and required in large quantity, which will significantly compromise the safety advantage of aqueous electrolyte.

Water-in-salt electrolytes (WiSEs) are another emerging strategy to reduce water reactivity to boost zinc metal anode reversibility [11]. The

* Corresponding author at: Helmholtz Institute Ulm (HIU), Helmholtzstrasse 11, D-89081 Ulm, Germany.
** Corresponding author at: Helmholtz Institute Ulm (HIU), Helmholtzstrasse 11, D-89081 Ulm, Germany.
E-mail addresses: fuhua.yang@kit.edu (F. Yang), alberto.varzi@kit.edu (A. Varzi).

https://doi.org/10.1016/j.cej.2024.157842
Received 5 September 2024; Received in revised form 4 November 2024; Accepted 18 November 2024
Available online 20 November 2024

high anions population forces them into the vicinity of Zn^{2+} to form close ion pairs that significantly exclude water molecules from the Zn^{2+} solvation shell. Examples of WiSEs for ZMB include $ZnCl_2$, water-in-bisalts electrolytes involving imide-based [12], acetate-based [13] and perchlorate-based electrolytes [14]. On the other hand, WiSEs require large quantity of (potentially) expensive zinc salt, thus, improved electrochemical performance is achieved only at high costs. In addition, the high viscosity and low ionic conductivity of WiSEs leads to high overpotentials and poor rate performance [4,15]. Thus, it is still challenging to effectively minimize solvated water in aqueous Zn-based electrolytes without significantly compromising their intrinsic advantages of low-cost, safety and high ionic conductivity.

In this work, a moderate concentration electrolyte with non-flammable components is developed to control the Zn^{2+} solvation structure. Specifically, trimethyl phosphate (TMP) is proposed as co-solvent in an acetate-based mixture of 1 m $ZnAc_2$ and 5 m KAc. TMP had been already studied as coordination agent for Zn ions but, in most cases, in combination with zinc triflate or perchlorate [2,16–18]. The presence of synergistic effects with salts based on hydrophilic anions such as acetate, that can coordinate both water and Zn^{2+}, has not been investigated so far. In our case, the addition of 5 m KAc increases the population of Ac anions in the electrolyte, as a result, Ac anions coordinate with the Zn^{2+} and the solvated water molecules in the inner solvation shell is reduced. Additionally, the flame-retardant TMP co-solvent not only takes part in the Zn^{2+} solvation shell, but also interrupts the H-bond network. Due to the synergistic effect of the salt anions and co-solvent molecules on the Zn^{2+} solvation structure, the solvated water is significantly minimized in the electrolyte, suppressing H_2 evolution and parasitic corrosion reaction of the zinc metal anode. Since acetate salts are low cost (see **Figure S1**) and eco-friendly [4,19], and only modest amounts of salts (1 m $ZnAc_2$ and 5 m KAc) and cosolvent (20 % in volume) are employed, it is expected that the production cost of the designed electrolyte is relatively low. Further post-mortem investigation on the Zn anode after cycling and modelling of the solvation structure of the electrolyte confirm the stability of the electrolyte towards H_2 evolution. The as-designed electrolyte enables prolonged cycling lifespan of more than 1500 h in Zn||Zn symmetrical cells. Finally, Zn||I_2 full cells exhibit improved cycling stability of 6000 cycles in acetated-based electrolytes with the addition of 20 % of TMP.

2. Results and discussion

The concentration of zinc acetate ($ZnAc_2$) and potassium acetate (KAc) in the electrolyte was fixed to 1 m and 5 m (denoted as 1Z5K), respectively. To understand the influence of TMP addition on the physico-chemical properties of the electrolytes, aqueous-organic hybrid solutions with TMP volume ratios of 20 % and 40 % (with respect to H_2O) were prepared and denoted as 8W2T and 6W4T, respectively. Fourier Transform Infrared spectroscopy (FTIR) measurements were firstly carried out to gain insight into the molecular interactions. As shown in Fig. 1**a**, the spectra feature the typical absorption peak in the 2600 to 3750 cm^{-1} regions ascribed to OH stretching of water molecules [17]. Interestingly, the peak experiences an obvious blueshift upon increasing the TMP content in the electrolyte. This suggests the formation of H-bonds between water and the multiple H-bond acceptors within the TMP molecule [17,20,21]. Fig. 1**b** displays the Raman spectra of various electrolytes and solvents within the range of 3100 to 3800 cm^{-1} (O-H stretching region) [4]. The spectra in this region were

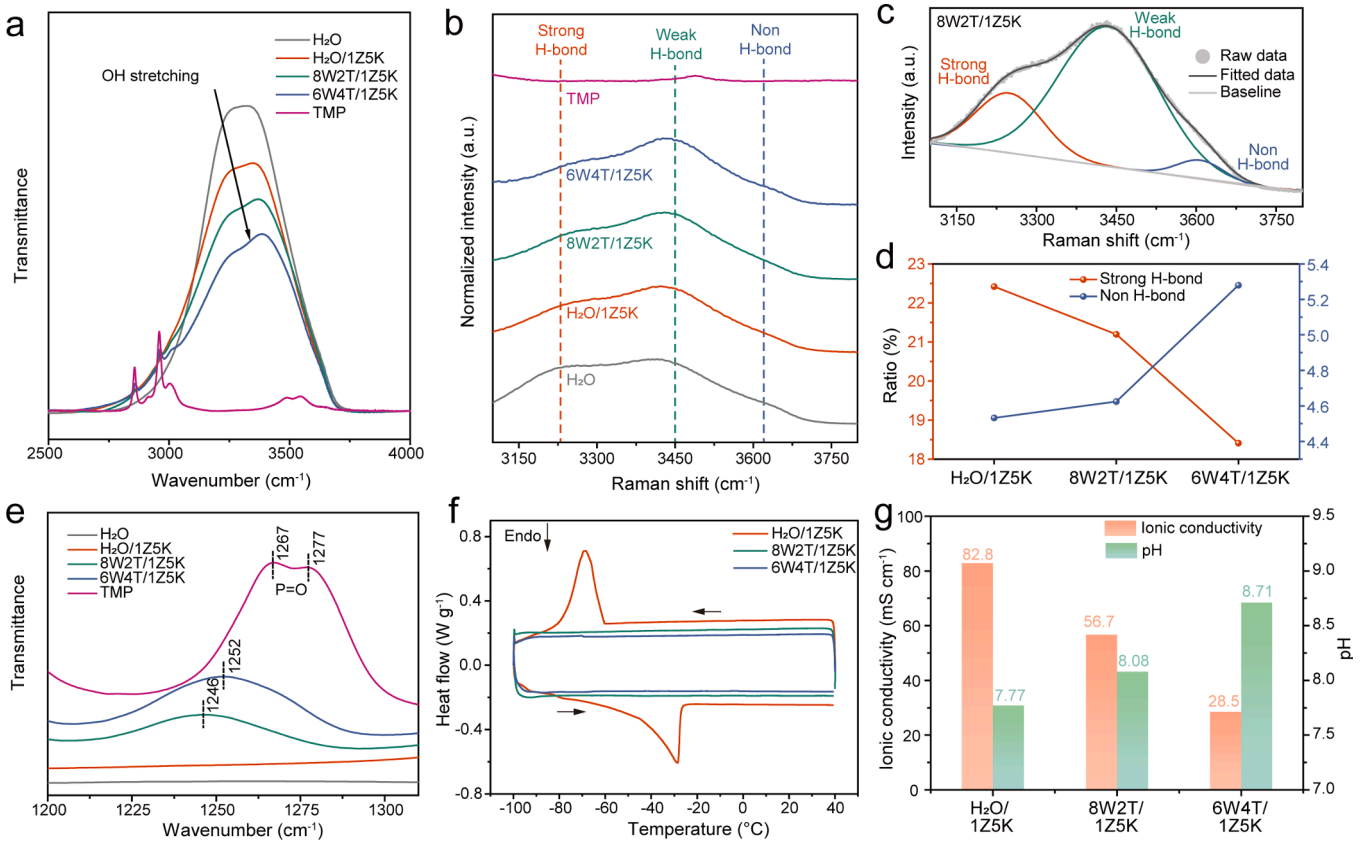

Fig. 1. Physico-chemical characterizations of the aqueous-TMP hybrid electrolytes with varying water:TMP volume ratio. (a) FTIR spectra and (b) Raman spectra of the electrolytes in the region of O-H stretching, including pure water and TMP solvents as reference. (c) Fitted O-H stretching vibrations of 8W2T/1Z5K. (d) Ratio of strong H-bond and non-H-bond in different electrolytes as a function of TMP concentration. (e) FTIR spectra of the electrolytes in the region of P = O vibration, including pure water and TMP solvents as reference (f) DSC curves of the different electrolytes upon cooling and heating (heating rate: 5 K min^{-1}). (g) Ionic conductivity and pH value of different electrolytes at 20 °C.

deconvoluted into three peaks to investigate the H-bonds variation as TMP content increases (see Fig. 1**c and Figure S2**). The three peaks refer to strong, weak and non-H-bonds [22] and the ratio of strong and non-H-bonds was also calculated as shown in Fig. 1**d**. Notably, as the TMP concentration was increased from 0 % to 40 %, the percentage of strong H-bonds obviously decreased, while that of non-H-bonds increased, evidencing the impact of TMP on the interruption of H-bonds. Fig. 1**e** shows the selected FTIR spectra in the range of 1200 to 1340 cm^{-1}, where features associated with P = O vibration can be observed [23]. As already reported in literature, the P = O vibration in pure TMP results in two separated peaks which are assigned to the two conformers [24], located at 1267 and 1277 cm^{-1}, respectively. However, only one peak ascribed to P = O is observed in the spectra of 8W2T/1Z5K and 6W4T/1Z5K hybrid electrolytes, possibly suggesting that only one conformer exists when the O atom in P = O coordinates the Lewis acids (Zn^{2+} and K^{+}). Furthermore, a considerable shift to lower wavenumbers is observed compared to pure TMP. The P = O peak in 8W2T/1Z5K demonstrates a more pronounced redshift compared to the other hybrid electrolyte of 6W4T/1Z5K (to 1246 cm^{-1} and 1252 cm^{-1}, respectively) indicating that the O in P = O has a stronger interaction with metallic cations [20]. Since there are two cations in these hybrid electrolytes (Zn^{2+} and K^{+}), the spectrum of the Zn-free 8W2T/5K (i.e. 5 m KAc) electrolyte was collected as well (see **Figure S3**). The location of the P = O vibration peak in 8W2T/5K is 1250 cm^{-1}, which is higher than that in 8W2T/1Z5K, implying that the O in P = O bond preferentially solvates Zn^{2+} rather than K^{+} ions. In order to further substantiate this claim, the FTIR analysis of P = O vibration in 8W2T/1 m $ZnAc_2$ electrolyte was conducted as well. As shown in **Figure S3b**, the wavenumber (1238 cm^{-1}) of the P = O vibration in 8W2T/1 m $ZnAc_2$ solution exhibits the most pronounced redshift compared to other solutions (1246 cm^{-1} in 8W2T/1Z5K and 1250 cm^{-1} in 8W2T/5 m KAc), corroborating that the O in P = O bond preferentially solvates Zn^{2+} rather than K^{+} ions.

DSC measurements were carried out to further reveal the influence of TMP on the disruption of H-bond networks in electrolytes (Fig. 1**f**). The electrolytes were first cooled down to −100 °C before heating to 40 °C. During this process, the heat flow was tracked to determine the freezing and melting point of the electrolytes. As expected, the H_2O/1Z5K electrolyte displays a substantial depression of the freezing point compared to pure water, due to the H-bond network perturbation by the acetate salts [25]. However, no melting point could be observed in both 8W2T/1Z5K and 6W4T/1Z5K electrolytes between −100 °C and 40 °C, suggesting for the excellent freezing resistance of the TMP-containing hybrid electrolytes [26]. To investigate the impact on the ionic transport, the ionic conductivity of the as-prepared electrolytes was determined at 20 °C, as shown in Fig. 1**g**. The ionic conductivity of H_2O/1Z5K is the highest, 82.8 mS cm^{-1}, and decreased when gradually replacing water with TMP, to 56.7 mS cm^{-1} for 8W2T/1Z5K and 28.5 mS cm^{-1} for 6W4T/1Z5K.

It is well established that the zinc anode reaction mechanism is determined by the pH of the electrolyte. In fact, in alkaline environment, $Zn(OH)_4^{2-}$ will decompose into insoluble ZnO, leading to shape change and passivation of the zinc metal anode [13,27]. In this regard, pH values of the various electrolytes and solvents were determined. As shown in **Table S1**, the pH value of pure (deionized, milliQ) water is slightly acidic. This is quite reasonable and caused by the dissolved CO_2 forming carbonic acid. The pH decreases substantially by addition of TMP, which is quite unexpected since TMP does not possess acidic protons. We do not currently have a reasonable explanation for this. At the moment, we could only speculate that TMP may promote CO_2 solubility [28] and, thus, formation of more carbonic acid. After addition of the acetate salts to the above solvents/mixtures, the pH value increased in all cases. In H_2O/1Z5K the pH increase caused by the hydrolysis of abundant acetate anions (since acetic acid is a weak acid) is sufficient to neutralize the carbonic acid, leading to a mildly alkaline environment (pH = 7.77). When decreasing the water fraction from 100 to 80 and 60 vol%, although the salt molality was constant (calculated on total mass of the solvent), the concentration of acetate salts with respect to water increased, leading to increased pH value in 8W2T/1Z5K (pH = 8.08) and 6W4T/1Z5K (pH = 8.71) compared to H_2O/1Z5K. Given that the major reaction mechanism between Zn electrodes in WiSE (1 m $ZnAc_2$ + 31 m KAc) with a pH value of 9.76 (limited amount of OH^- ions, 6×10^{-5} mol/L) was confirmed to be Zn stripping/plating [13], it is reasonable to conclude that the Zn metal anode in these hybrid electrolytes with a lower OH^- concentration can still undergo reversible Zn stripping/plating ($Zn \rightleftharpoons Zn^{2+} + 2e^-$).

According to our previous work, Zn metal suffers from severe corrosion in medium/low-concentration acetate-based electrolytes [19]. To investigate the effect of TMP on Zn corrosion, linear polarization measurements of Zn electrodes and post-mortem analysis of soaked Zn electrodes were carried out. Fig. 2**a** shows the Tafel plot within the voltage range of −0.8 to −1.1 V (vs. Ag/AgCl) at a scan rate of 5 mV/s. The exchange current densities of Zn electrodes in H_2O/1Z5K, 8W2T/1Z5K and 6W4T/1Z5K are 2.601, 0.368 and 0.154 mA cm^{-2}, respectively. The relatively low values evidence minimized corrosion in TMP containing electrolytes. Zn metal foils were also immersed in 1.0 mL of electrolyte for 14 days before being subject to XRD measurements to evidence corrosion products. As shown in Fig. 2**b**, apart from the Zn characteristic features, other peaks ascribed to side products, e.g., ZnO, $Zn(OH)_2$ and $Zn_5(CO_3)_2(OH)_6$, are observed for the zinc metal stored in H_2O/1Z5K, indicating severe corrosion [19]. In contrast, the XRD patterns of Zn foil after soaking in 8W2T/1Z5K and 6W4T/1Z5K only present the fingerprints of pure Zn metal. SEM measurements were also carried out on the same samples. Loose and uneven flake-shape features ascribed to the corrosion products are observed on the surface of the Zn foil stored in H_2O/1Z5K (Fig. 2**c**). Whereas the samples in prolonged contact with 8W2T/1Z5K (Fig. 2**d**) and 6W4T/1Z5K (Fig. 2**e**) display flat and dense surface resulting from the excellent corrosion resistance imparted by TMP.

To evaluate the impact of the different electrolytes on the Zn metal anode electrochemical performance, Zn||Zn symmetrical cells were subject to galvanostatic plating/stripping tests. Fig. 3**a** shows the long-term plating/stripping behavior of symmetrical cells at a current density of 2 mA cm^{-2}. These cells were initially activated at lower current density (0.5 mA cm^{-2}, 0.5 mAh cm^{-2}) for 3 cycles. Zn||Zn symmetrical cells with H_2O/1Z5K were able to reach a cycling life of 140 h before short circuit occurred. On the contrary, the symmetrical cells with 6W4T/1Z5K and 8W2T/1Z5K display stable voltage profiles for over 360 and 1500 h, respectively. By comparing the long-term cycling stability of symmetric cells in various organic/water hybrid electrolytes (**Table S2**), the performance obtained with the 8W2T/1Z5K electrolyte can be considered excellent. It should be noted, however, that a larger polarization is observed for the TMP-added electrolytes. The higher the TMP volume ratio, the larger is the polarization (see **Figure S4**). This can obviously be correlated to the lower ionic conductivity of the electrolytes. Additionally, we cannot exclude that the solvation of Zn^{2+} by TMP may play a role as well [29]. To further investigate the influence of TMP addition during Zn deposition, 2.0 mAh cm^{-2} of Zn were plated on Zn substrates in H_2O/1Z5K and 8W2T/1Z5K electrolytes. When compared to the pristine Zn electrodes (**Figure S5a-b**), inhomogeneous and loose deposits in H_2O/1Z5K electrolyte occurred (see **Figure S5c-d**). However, in the case of 8W2T/1Z5K electrolyte, the morphology of deposited Zn was quite compact with large Zn crystals as it can be seen from **Figure S5e-f**. These results indicate that 20 vol% of TMP addition could effectively induce the uniform and dense deposition of Zn, which is beneficial to the long-term cycling performance of Zn metal anodes and is consistent with the foregoing outstanding electrochemical performance of symmetrical cells in 8W2T/1Z5K electrolyte. Thus, 8W2T/1Z5K electrolyte was chosen to further test the long-term stability of symmetrical cells at a higher areal capacity (5 mAh cm^{-2}), displaying a lifespan of 180 h (see **Figure S6**).

As shown in Fig. 3**b**, the rate performance of symmetrical cells was also evaluated at different current densities of 0.5, 1, 2, 4, 5 and 8 mA

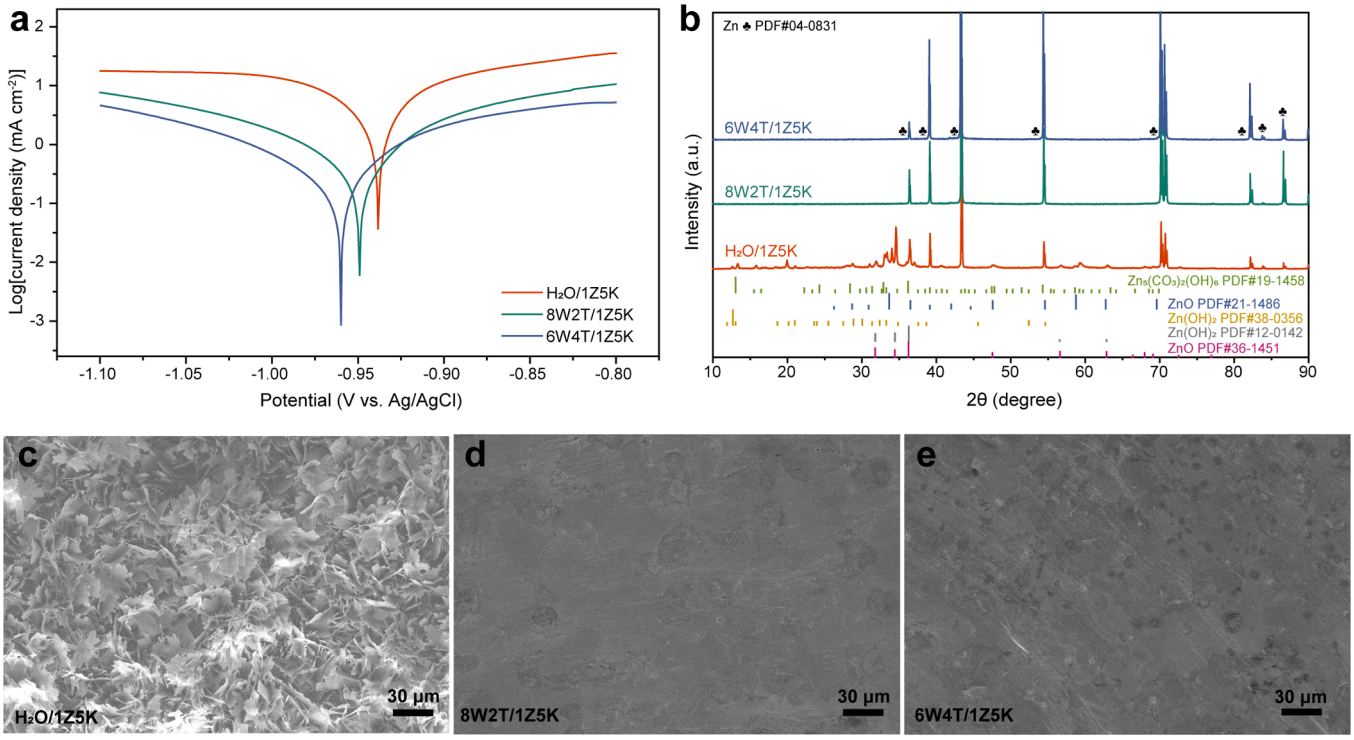

Fig. 2. (a) Linear polarization (Tafel) curves of Zn electrodes in different electrolytes at a scan rate of 5 mV/s, employing Zn foil as the counter electrode and leakless Ag/AgCl electrode as reference electrode. (b) XRD pattern of Zn foils after a 14-day immersion into H_2O/1Z5K, 8W2T/1Z5K and 6W4T/1Z5K, respectively. SEM images of the soaked Zn in (c) H_2O/1Z5K, (d) 8W2T/1Z5K and (e) 6W4T/1Z5K.

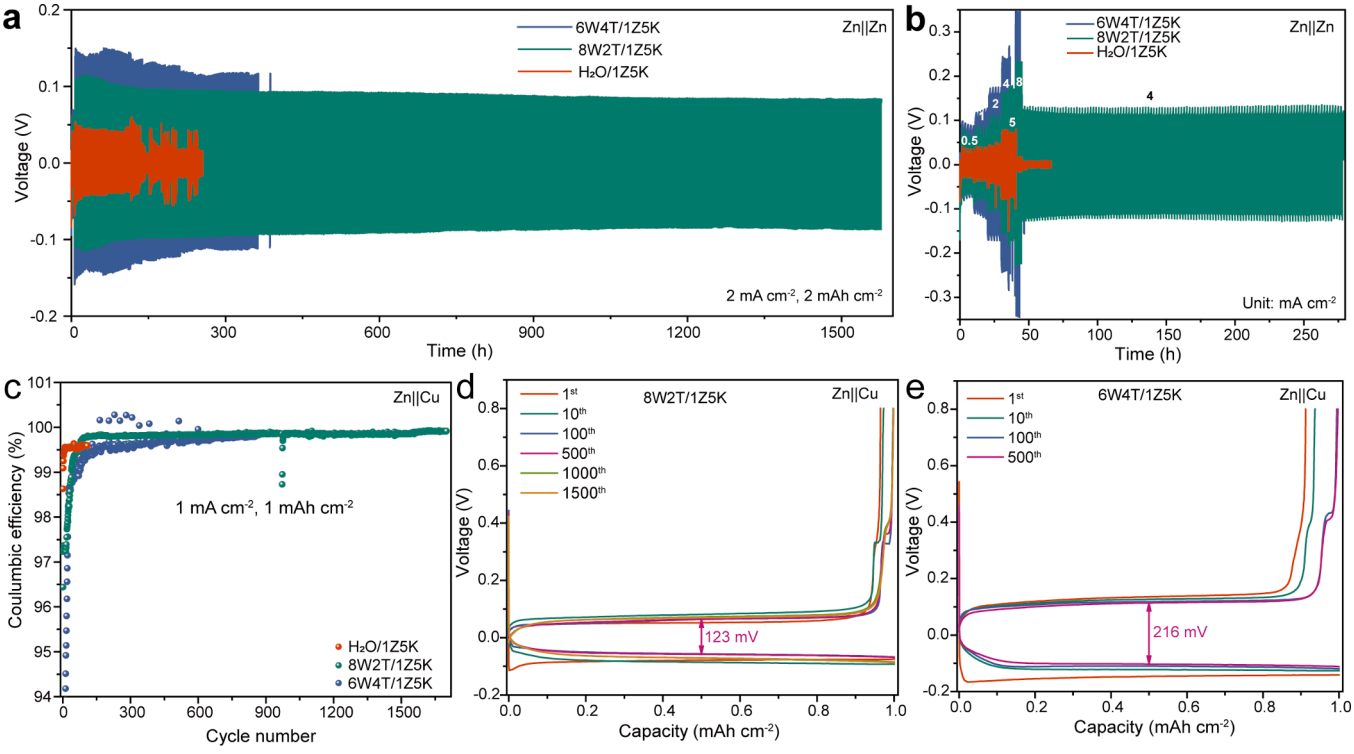

Fig. 3. (a) Long-term galvanostatic stripping/plating tests of symmetrical Zn cells in different electrolytes at a current density of 2.0 mA cm^{-2} (1 h each step). (b) Stripping/plating voltage of symmetrical Zn cells under different current densities. (c) The CE evolution of Zn||Cu cells in different electrolytes upon long-term cycling at current density of 1.0 mA cm^{-2}. The corresponding voltage profiles of asymmetric Zn||Cu cells in (d) 8W2T/1Z5K and (e) 6W4T/1Z5K electrolytes.

cm^{-2}. For better visualization, the portion of the figure showing the voltage profiles at different currents has been enlarged (see **Figure S7**). As current densities increased, the polarization observed in the TMP-added hybrid electrolytes became more pronounced. Nevertheless, the symmetrical cell with 8W2T/1Z5K still demonstrated the best electrochemical performance, since stable stripping/plating behavior was achieved under 8 mA cm^{-2}, followed by further stable cycling at 4 mA cm^{-2} (a fixed plating/stripping capacity of 4 mAh cm^{-2}) for over 230 h. At the even higher current density of 8 mA cm^{-2}, the cell with H_2O/1Z5K suffered from short-circuit likely due to dendrite growth. The cell with 6W4T/1Z5K could not withstand such high currents due to the slowest ion diffusion rate of the electrolyte [30].

Zn||Cu cells were also tested to evaluate the reversibility of Zn plating/stripping process. The voltage profiles upon the first plating step in the three electrolytes are displayed and compared in **Figure S5a-c**. There are two characteristic overpotentials during the first plating process: nucleation overpotential (η_n) and growth overpotential (η_g). The former is associated with the nucleation of Zn seeds. As **Figure S8** shows, the nucleation overpotential increases as the TMP concentration increases. The larger the η_n is, the greater number of nuclei on the substrate is formed, indicating that the addition of TMP could help with the formation of more and smaller nuclei [31]. On the other hand, the η_g overpotential also suggests for higher energy barrier for subsequent Zn growth in the presence of TMP. The deposition capacity in the test was fixed at 1 mAh cm^{-2}, implying that a smaller portion of Zn was deposited on each nucleus if the number of the nuclei is larger. As a result, denser Zn nuclei in TMP-containing electrolytes are expected, which reduce the risk of dendrite growth. Afterwards, the long-term CE evolution was evaluated, which is a crucial indicator for the reversibility of metal [32]. As Fig. 3**c** shows, the Zn||Cu cell with 8W2T/1Z5K displays the longest lifespan of 1700 cycles with a CE over 99.7 %, while the Zn||Cu cells with H_2O/1Z5K failed after only 109 cycles (**Figure S8d**), possibly due to dendrite growth, achieving a CE of 99.5 %. Furthermore, the comparison of voltage profiles of asymmetric Zn||Cu cells with different TMP additions is shown in Fig. 3**d-e**. The asymmetric Zn||Cu cell with 8W2T/1Z5K always presented smaller polarization (123 mV at the 500th cycle) than that with 6W4T/1Z5K (216 mV at the 500th cycle). In summary, 8W2T/1Z5K outperformed both H_2O/1Z5K and 6W4T/1Z5K, and was selected for further investigation.

Before proceeding further, in order to highlight advantages of this novel TMP-acetate combination, further tests were performed with a control solution with the same composition but based on triflate. In fact, as mentioned before, TMP had been already studied as coordination agent for Zn ions but, in most cases, in combination with zinc triflate. Thus, the electrolyte 1 m $ZnOTf_2$ + 5 m KOTf in 8W2T (denoted as 8W2T/1Z5K-triflate) was prepared and compared with 8W2T/1Z5K to highlight the unique advantages of the TMP-acetate synergy. First of all, the lower cost is a non-negligible advantage of the acetate-based electrolyte compared to the triflate-based counterpart (see **Figure S1**). Additionally, the electrochemical performances of symmetrical Zn||Zn and asymmetrical Zn||Cu cells were also tested in 8W2T/1Z5K-triflate under the same conditions as in 8W2T/1Z5K. As shown in **Figure S9a**, despite showing a smaller polarization compared to 8W2T/1Z5K, symmetrical cells with 8W2T/1Z5K-triflate were only able to reach a cycling life of 40h before experiencing a short circuit. To further investigate the influence of 8W2T/1Z5K-triflate electrolyte during Zn deposition, 2.0 mAh cm^{-2} of Zn were plated on Zn substrates. As **Figure S9b-c** shows, Zn deposits were unevenly distributed and easily embedded in the glass fiber separator, revealing the reason for the short lifespan being dendrite growth. Particularly, a restricted deposition area was observed as shown in the insert optical image of Zn electrode, suggesting that 8W2T/1Z5K-triflate electrolyte exhibits worse interfacial compatibility, which is evidenced also by the large nucleation overpotential observed in the first cycle (−0.284 V) in **Figure S9a**. Afterwards, Zn||Cu cells were tested to evaluate the reversibility of Zn plating/stripping process (see **Figure S9d**). The average CE of Zn||Cu cell in 8W2T/1Z5K-trifalte electrolyte is 98.9 %, which is much lower than 8W2T/1Z5K electrolyte (99.7 %), possibly resulting from a more intense H_2 evolution and its associated side reactions. The nucleation overpotential of Zn deposition on Cu is also larger in 8W2T/1Z5K-triflate (see **Figure S9e**) than 8W2T/1Z5K (see **Figure S8b**).

Afterwards, Zn electrodes after 50 cycles in the acetate electrolytes were further investigated by SEM, XPS and XRD, respectively, to reveal the surface morphology and chemistry. The morphological changes are evident. Compared to the original Zn foils in **Figure S5a-b**, Zn electrodes, after cycling in H_2O/1Z5K show a loose and rough surface, which may partially be ascribed to the not uniform Zn deposits and side-products (see **Figure S10a-b**) [33]. Furthermore, the clearly larger surface area may favor H_2 evolution, which is detrimental to the long-term cycling of Zn electrodes, as previously shown in Fig. 3**a-b** [34]. Differently, the surface of Zn metal electrode cycled in 8W2T/1Z5K displays dense and uniform morphology with no clear sign of side products, as shown in **Figure S10c-d**.

The presence of side-products on the Zn metal electrode surfaces was further investigated by XPS. The Zn $2p_{3/2}$ spectra taken at the Zn electrode surface cycled in H_2O/1Z5K electrolyte (Fig. 4**a**) show one feature at 1022.48 eV, while the Zn electrode tested in 8W2T/1Z5K (Fig. 4**b**) displayed two distinguished peaks at 1021.4 and 1022.9 eV. The species observed in the Zn $2p_{3/2}$ region exhibit small chemical shifts, which might result from charging effects. Therefore, the Zn Auger parameters (α_{Zn} − the sum of the Zn $2p_{3/2}$ binding energy and the Zn_{LMM} kinetic energy) were calculated to assign the observed peaks to the corresponding species (note that this approach is the best method for identifying metal-based species) [35]. The surface species on the Zn electrode tested in H_2O/1Z5K (at 1022.48 eV) can be assigned to $Zn_5(CO_3)_2(OH)_6$ and/or $ZnCO_3$ (α_{Zn} = 2009.7 ± 0.2 eV) [36], in agreement with XRD results. According to literature, the CO_3^{2-} species in $Zn_5(CO_3)_2(OH)_6$ derived from the atmospheric CO_2 naturally dissolved in the electrolyte. During Zn deposition, H_2 evolution reaction takes place near the Zn surface in H_2O/1Z5K electrolyte and then the local pH increases. Consequently, CO_3^{2-} and OH^- combine with Zn^{2+} to form $Zn_5(CO_3)_2(OH)_6$ [37]. Meanwhile, the surface species observed for the Zn electrodes cycled in 8W2T/1Z5K correspond to Zn metal (α_{Zn} = 2012.9 ± 0.2 eV) and ZnO (α_{Zn} = 2010.6 ± 0.2 eV) [36], confirming the suppression of the Zn electrode corrosion by addition of TMP. The depth profiling of the Zn electrodes was also performed. While both Zn electrodes exhibit the presence of Zn metal and ZnO at 8 nm underneath the outer surface, the Zn electrode tested in 8W2T/1Z5K displays a much more homogeneous composition. In addition, the O 1s spectra of Zn electrodes tested in H_2O/1Z5K and 8W2T/1Z5K confirmed the higher reactivity and inhomogeneous surface of the Zn metal cycled in H_2O/1Z5K electrolyte. The Zn electrode tested in H_2O/1Z5K exhibits the characteristic features of the –OH, –C = O and –COOR bonds corresponding to Zn(OH), $ZnCO_3$, and/or $Zn_5(CO_3)_2(OH)_6$ decomposition products and acetate-electrolyte traces (−COOK and −COK), while at higher depths the presence of ZnO is clearly evidenced, in agreement with Zn $2p_{3/2}$. Meanwhile, the Zn electrode cycled in 8W2T/1Z5K is covered by ZnO and residues of the acetate salts (−COOK and −COK). The C 1s region has also been analyzed (**Figure S11**), and the results are in agreement with the O 1s spectra, displaying the presence of hydrocarbons (C-C/C-H), −C = O/-COK and −COOR/-COOK groups from decomposition products and acetate electrolyte leftovers [38]. Finally, the Zn electrode cycled in 8W2T/1Z5K does not show any P-containing species (**Figure S12**), indicating that the TMP is most probably not contributing to the formation of any interphase in this electrolyte. XRD patterns were also collected to further reveal the crystallographic properties of the Zn electrodes after cycling. As shown in **Figure S13**, the XRD pattern of bare Zn are displayed as reference. Unfortunately, no clear fingerprints of side products (such as $Zn_5(CO_3)_2(OH)_6$) could be detected on Zn electrodes cycled in H_2O/1Z5K by means of XRD. This is probably due to the relatively short cycling time (50 cycles, 5 days). Interestingly, though, the intensity ratio of $I_{(002)}/I_{(101)}$ decreased

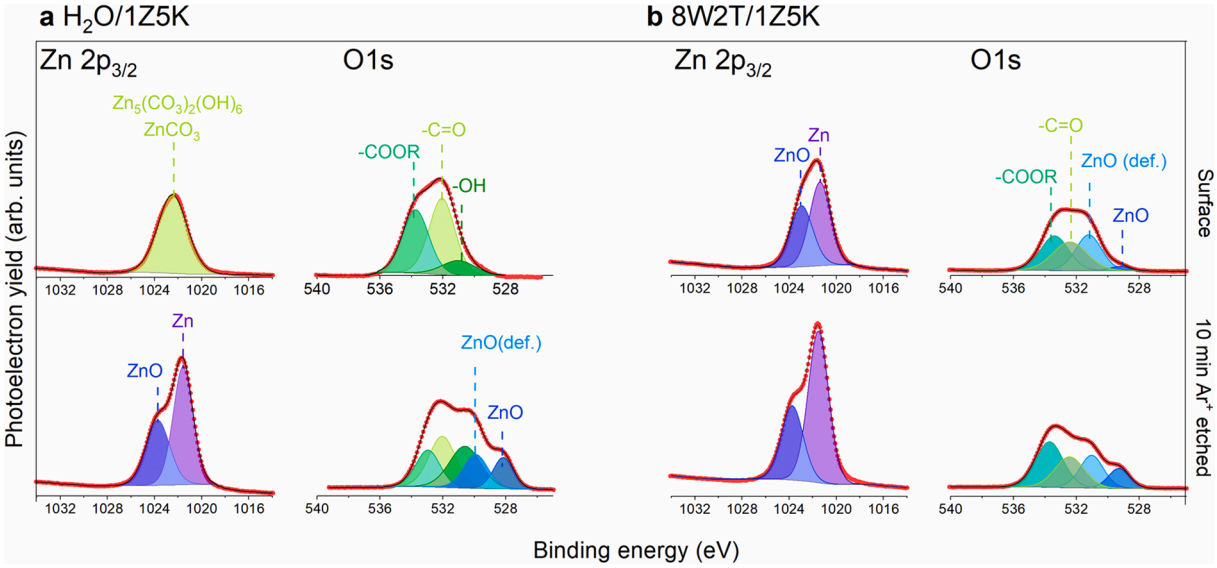

Fig. 4. XPS spectra (Zn $2p_{3/2}$ and O 1s) taken at the surface and 8 nm deep into Zn electrodes cycled in (a) H_2O/1Z5K and (b) 8W2T/1Z5K.

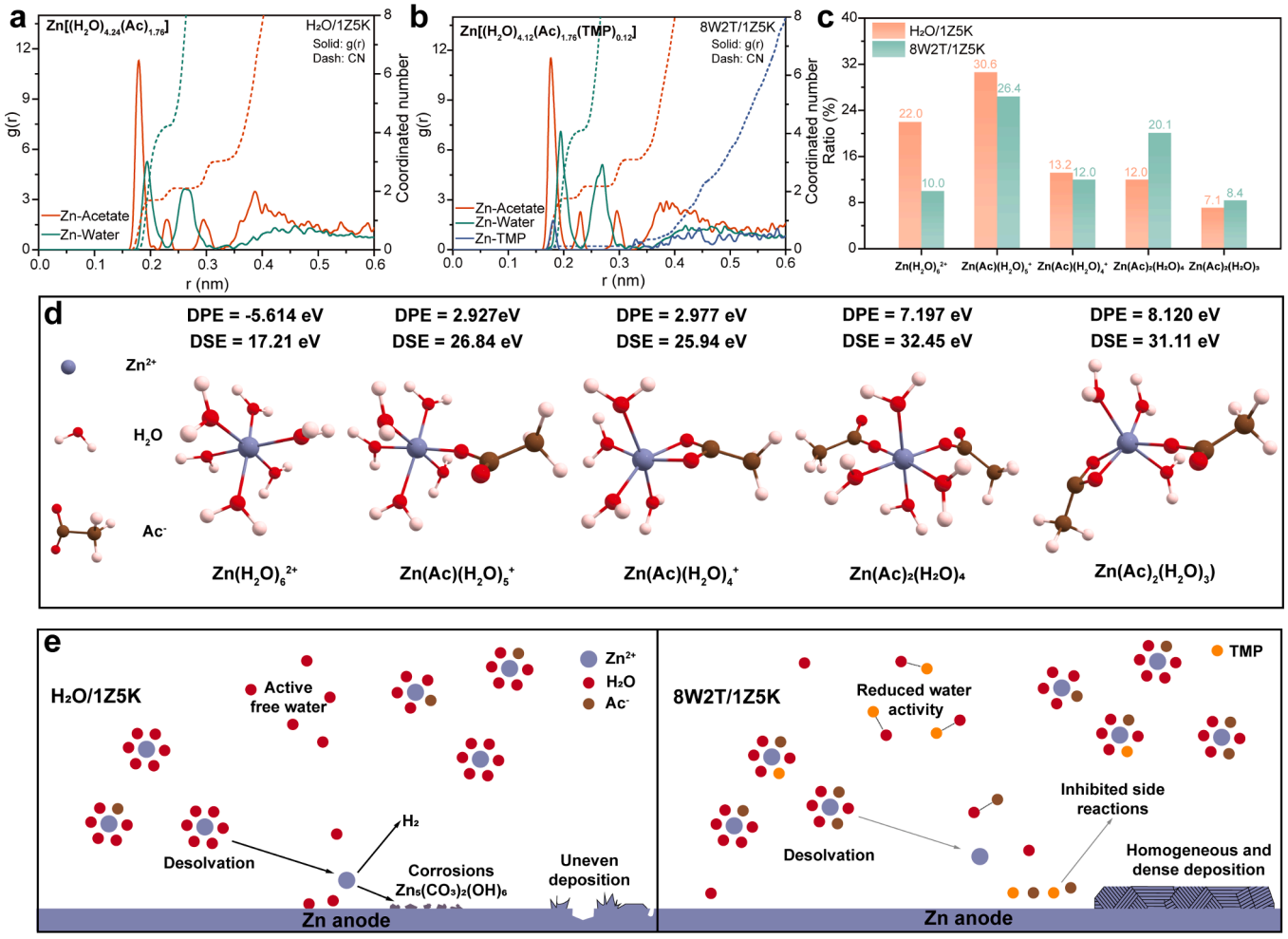

Fig. 5. RDFs for Zn-acetate, Zn-water and Zn-TMP pairs in (a) H_2O/1Z5K and (b) 8W2T/1Z5K. (c) Population comparison of the top five complex structures by concentration ($Zn(H_2O)_6^{2+}$, $Zn(Ac)(H_2O)_5^{+}$, $Zn(Ac)(H_2O)_4^{+}$, $Zn(Ac)_2(H_2O)_4$ and $Zn(Ac)_2(H_2O)_3$) of Zn^{2+} inner solvation shell in two electrolytes. (d) Representative structures of Zn^{2+} inner solvation shell in both electrolytes and their deprotonation (H^+ dissociation of H_2O) energy from Zn^{2+} inner solvation shell and de-solvation energy. (e) Schematic illustration of the different processes, Zn-ion solvation shell and surface evolution of Zn electrodes in H_2O/1Z5K and 8W2T/1Z5K electrolytes.

compared to bare Zn. According to the literature, the crystallographic planes (101) and (002) correspond to the vertical and horizontal alignment of Zn crystal, respectively [39]. The (101) plane evidence dendrite growth which exacerbate Zn corrosion, whereas the (002) plane suggests more compact deposits during Zn deposition which provide higher resistance to corrosion [40]. In the case of Zn electrodes cycled in 8W2T/1Z5K electrolyte, the intensity ratio of $I_{(002)}/I_{(101)}$ substantially increases, which is in line with the improved stability upon cycling.

Molecular Dynamics (MD) simulations were further conducted to explore the solvation structure of H_2O/1Z5K and 8W2T/1Z5K electrolytes. Radial Distribution Functions (RDFs) calculated the distribution of the nearest-neighbor molecules around a reference Zn^{2+}, as shown in Fig. 5**a-b**. The coordination number for both electrolytes is the same (six), including 4.24 water molecules, and 1.76 acetate anions in H_2O/1Z5K and 4.12 water molecules, 1.76 acetate anions and 0.12 TMP molecules in 8W2T/1Z5K electrolyte, based on the statistical findings. Even though TMP appears to have little influence on the Zn^{2+} inner solvation structures, which may explain the disappearance of P-based species on Zn surface in XPS results, the addition of TMP showed a substantial impact on the distribution of Zn^{2+} solvation structures. The concentration (more than 1 %) of different Zn^{2+} inner solvation shells in H_2O/1Z5K and 8W2T/1Z5K are summarized in **Tables S3 and S4**, respectively. The top 5 species by concentration are displayed in Fig. 5**c**, demonstrating that the addition of TMP reduces the concentration of $Zn(H_2O)_6^{2+}$ and increases the concentration of $Zn(Ac)_2(H_2O)_4$. Furthermore, the deprotonation energy (DPE) of solvated water in the 5 species are plotted in Fig. 5**d**. $Zn(H_2O)_6^{2+}$ has the lowest DPE, underscoring deprotonation of solvated H_2O is the most energetically favourable [8]. Some selective solvation structure of Zn^{2+} are also displayed in **Figure S14**. These results indicate that the solvated H_2O impact is reduced in the TMP-regulated solvation structure, thus suppressing parasitic reactions including H_2 evolution [8], which is consistent with the former experimental results. In addition, the de-solvation energies (denoted as DSE) of the solvate molecules from Zn^{2+} inner solvation shell were calculated as well (see Fig. 5d). $Zn(H_2O)_6^{2+}$ has the lowest DSE of 17.21 eV among the various complex structure which means the de-solvation process during Zn deposition is the most energetically favorable. In contrary, the highest DSE (32.45 eV) was observed from Zn $(Ac)_2(H_2O)_4$ complex, confirming the higher polarization of symmetrical cells in 8W2T/1Z5K electrolyte by comparison of the distribution of Zn-complex in both cases. According to the above discussions, the different factors enhancing the stability of Zn metal anode in 8W2T/1Z5K electrolyte can be summarized in Fig. 5**e**.

Finally, Zn||I_2 full cells were also assembled and subject to electrochemical testing to verify the feasibility of the designed electrolyte. For the cathode's preparation, a solution constituted by 1 M LiI and 0.1 M I_2 in H_2O was drop-casted onto a Ti-supported Ketjen black (KB) membrane. As shown by the CV in Fig. 6**a**, one typical pair of redox peaks associated with the I^-/I^0 conversion reaction is observed in H_2O/1Z5K electrolyte. However, there are clearly two reduction peaks indexed to $I_2 \rightarrow I_3^- \rightarrow I^-$ reaction in 8W2T/1Z5K while only one peak was observed ascribed to the I^-/I^0 conversion reaction during oxidation process [41]. The main redox peaks of the I_2 cathode in 8W2T/1Z5K was shifted of around 0.1 V towards lower potentials, indicating that the Zn^{2+} activity was suppressed after adding TMP [42]. Interestingly, the voltage difference between the cathodic and anodic peaks in both electrolytes is close, and a similar voltage polarization of 55 mV is observed for both electrolytes [43]. Afterwards, the rate performance and long-term cycling stability of full cells were evaluated, as presented in Fig. 6**b-c**. It is worth noting that the capacity delivered by the I_2 cathode in H_2O/1Z5K is always higher than that in 8W2T/1Z5K, at each current density. Additionally, the polarization in the galvanostatic charge/discharge (GCD) profiles in 8W2T/1Z5K (Fig. 6**e**) is larger than that in H_2O/1Z5K (Fig. 6**d**) at relatively higher current density (2.0 and 5.0 mA cm^{-2}) due to the lower ionic conductivity of the former electrolyte. Nevertheless, the cycle life of the full cell employing 8W2T/1Z5K is nearly twice as long than that in H_2O/1Z5K, achieving more than 6000 cycles. Additionally, the GCD profiles of the full cell with 8W2T/1Z5K did not display any increase in polarization upon cycling Fig. 6**f**. In the case of H_2O/1Z5K, a substantially increase irreversible capacity was observed after 2020 cycles (see **Figure S15**), which may be a sign of polyiodide

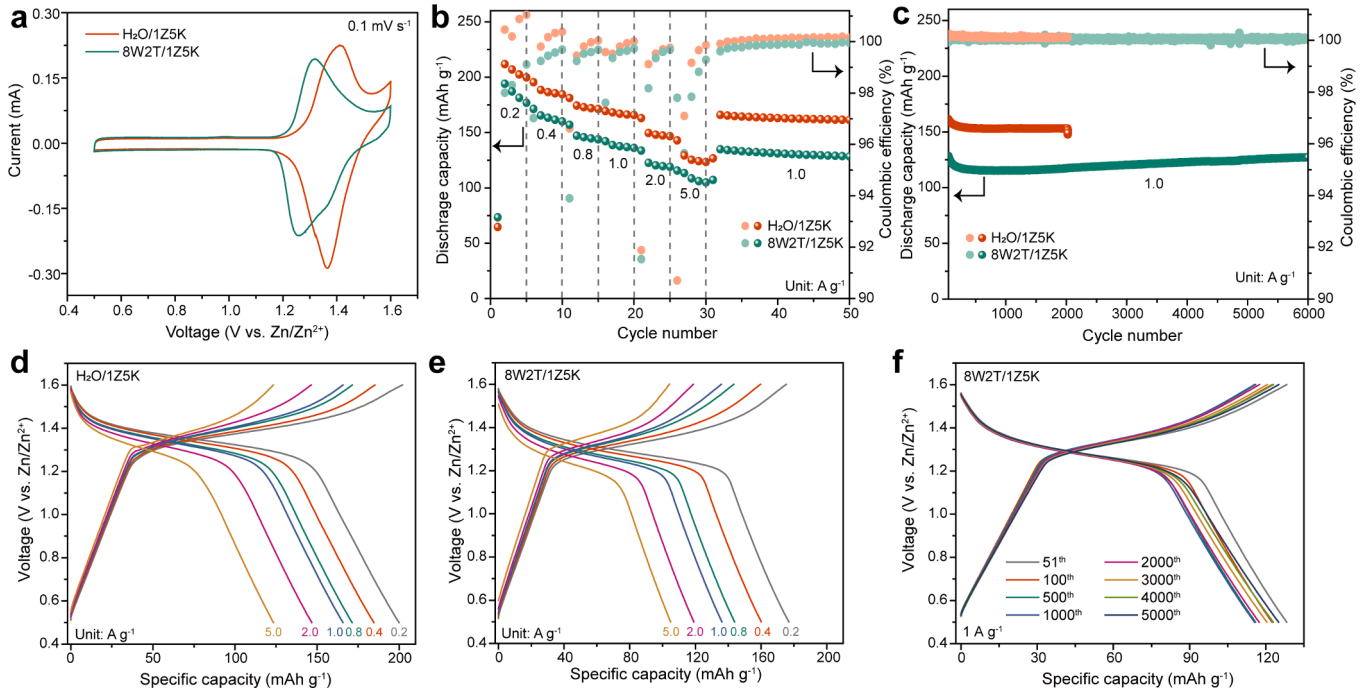

Fig. 6. Electrochemical performance of ZMBs with I_2 cathode. (a) CV curves, (b) rate performance under different current densities and (c) cycling performance at 1 A/g between 0.5 and 1.6 V of Zn||I_2 full cells in different electrolytes. GCD profiles of Zn||I_2 full cells in (d) H_2O/1Z5K and (e) 8W2T/1Z5K electrolytes at different current densities. (f) Selected GCD profiles of Zn||I_2 full in 8W2T/1Z5K electrolyte at current density of 1 A/g.

shuttling [43].

In order to gain some insight into the mechanism behind the different electrochemical performance of I_2 in the two electrolytes, identical amounts of polyiodides (containing 2 mg of I element) were added into the H_2O/1Z5K and 8W2T/1Z5K electrolytes. After the polyiodide addition, a purple precipitate, presumably being I_2, could be observed in the 8W2T/1Z5K electrolyte. In contrast, the H_2O/1Z5K electrolyte remained transparent (see **Figure S16**), suggesting that the TMP-containing 8W2T/1Z5K electrolyte features a limited polyiodide solubility, which is beneficial to suppress the "shuttle effect" of the Zn||I_2 batteries [43].

3. Conclusions

A hybrid aqueous-organic electrolyte with 1 m $ZnAc_2$ and 5 m KAc dissolved in the 80:20 water:TMP (v/v) mixture was developed for aqueous zinc ion batteries. The relatively high concentration of Ac^- anions and the presence of TMP not only interrupt the H-bond network of water, but also enable their participation in the Zn^{2+} solvation structure. As a result, H_2 evolution and associated corrosion reaction on zinc metal anode are suppressed. The as-designed 8W2T/1Z5K allowed an excellent cycling stability of 1570 h of Zn||Zn symmetrical cells as well as high average CE of 99.7 % in Zn||Cu asymmetrical cells over 1700 cycles. In addition, Zn||I_2 full cells in TMP-modified electrolytes achieved excellent long-term cycling performance (6,000 cycles), which is mainly attributed to the improved Zn anode reversibility and suppressed shuttle effect of polyiodide.

CRediT authorship contribution statement

Huifang Fei: Writing – original draft, Visualization, Validation, Methodology, Investigation, Funding acquisition, Formal analysis, Data curation, Conceptualization. **Fuhua Yang:** Writing – review & editing, Supervision, Methodology, Funding acquisition, Conceptualization. **Jodie A. Yuwono:** Software, Methodology, Investigation, Formal analysis. **Maider Zarrabeitia:** Writing – review & editing, Methodology, Investigation, Formal analysis, Data curation. **Stefano Passerini:** Writing – review & editing, Supervision. **Alberto Varzi:** Writing – review & editing, Supervision, Resources, Project administration, Funding acquisition, Conceptualization.

Declaration of competing interest

The authors declare that they have no known competing financial interests or personal relationships that could have appeared to influence the work reported in this paper.

Acknowledgements

H. Fei sincerely acknowledges the financial support from China Scholarship Council. F. Yang gratefully acknowledges the financial support from the Humboldt Foundation. J. Yuwono acknowledges the high-performance computing support provided by National Computational Infrastructure Australia. This work was financially supported by Federal Ministry of Education and Research (BMBF) within the ZILUBAT-NEU project (grant no. 03XP0488B). Financial support from the Helmholtz Association is also acknowledged by all the authors from HIU. We sincerely appreciate the support of Yao Qin from HIU for the Raman measurement.

Appendix A. Supplementary data

Supplementary data to this article can be found online at https://doi.org/10.1016/j.cej.2024.157842.

Data availability

Data will be made available on request.

References

[1] F. Duffner, N. Kronemeyer, J. Tübke, J. Leker, M. Winter, R. Schmuch, Post-lithium-ion battery cell production and its compatibility with lithium-ion cell production infrastructure, Nat. Energy 6 (2021) 123–134, https://doi.org/10.1038/s41560-020-00748-8.
[2] J. Janek, W.G. Zeier, Challenges in speeding up solid-state battery development, Nat. Energy 8 (2023) 230–240, https://doi.org/10.1038/s41560-023-01208-9.
[3] X. Zhang, H. Wei, S. Li, B. Ren, J. Jiang, G. Qu, H. Lv, G. Liang, G. Chen, C. Zhi, H. Li, Z. Liu, Manipulating coordination environment for a high-voltage aqueous copper-chlorine battery, Nat. Commun. 14 (2023) 6738, https://doi.org/10.1038/s41467-023-42549-z.
[4] D. Dong, T. Wang, Y. Sun, J. Fan, Y.-C. Lu, Hydrotropic solubilization of zinc acetates for sustainable aqueous battery electrolytes, Nat. Sustain. 6 (2023) 1474–1484, https://doi.org/10.1038/s41893-023-01172-y.
[5] Q. Ni, B. Kim, C. Wu, K. Kang, Non-electrode components for rechargeable aqueous zinc batteries: electrolytes, solid-electrolyte-interphase, current collectors, binders, and separators, Adv. Mater. 34 (2022) 2108206, https://doi.org/10.1002/adma.202108206.
[6] Q. Li, Y. Zhao, F. Mo, D. Wang, Q. Yang, Z. Huang, G. Liang, A. Chen, C. Zhi, Dendrites issues and advances in Zn anode for aqueous rechargeable Zn-based batteries, EcoMat 2 (2020) e12035, https://doi.org/10.1002/eom2.12035.
[7] G. Ma, S. Di, Y. Wang, W. Yuan, X. Ji, K. Qiu, M. Liu, X. Nie, N. Zhang, Zn metal anodes stabilized by an intrinsically safe, dilute, and hydrous organic electrolyte, Energy Storage Mater. 54 (2023) 276–283, https://doi.org/10.1016/j.ensm.2022.10.043.
[8] F. Yang, J.A. Yuwono, J. Hao, J. Long, L. Yuan, Y. Wang, S. Liu, Y. Fan, S. Zhao, K. Davey, Understanding H2 evolution electrochemistry to minimize solvated water impact on Zinc-anode performance, Adv. Mater. 34 (2022) 2206754, https://doi.org/10.1002/adma.202206754.
[9] B. Raza, A. Naveed, H. Lu, T. Rasheed, J. Yang, Y. NuLi, J. Wang, Zn anode sustaining high rate and high loading in organic electrolyte for rechargeable batteries, Energy Storage Mater. 46 (2022) 523–534, https://doi.org/10.1016/j.ensm.2022.01.043.
[10] L. Miao, R. Wang, S. Di, Z. Qian, L. Zhang, W. Xin, M. Liu, Z. Zhu, S. Chu, Y. Du, N. Zhang, Aqueous electrolytes with hydrophobic organic cosolvents for stabilizing zinc metal anodes, ACS Nano 16 (2022) 9667–9678, https://doi.org/10.1021/acsnano.2c02996.
[11] H. Yan, X. Zhang, Z. Yang, M. Xia, C. Xu, Y. Liu, H. Yu, L. Zhang, J. Shu, Insight into the electrolyte strategies for aqueous zinc ion batteries, Coord. Chem. Rev. 452 (2022) 214297, https://doi.org/10.1016/j.ccr.2021.214297.
[12] F. Wang, O. Borodin, T. Gao, X. Fan, W. Sun, F. Han, A. Faraone, J.A. Dura, K. Xu, C. Wang, Highly reversible zinc metal anode for aqueous batteries, Nat. Mater. 17 (2018) 543–549, https://doi.org/10.1038/s41563-018-0063-z.
[13] S. Chen, R. Lan, J. Humphreys, S. Tao, Salt-concentrated acetate electrolytes for a high voltage aqueous Zn/MnO_2 battery, Energy Storage Mater. 28 (2020) 205–215, https://doi.org/10.1016/j.ensm.2020.03.011.
[14] Y. Zhu, J. Yin, X. Zheng, A.-H. Emwas, Y. Lei, O.F. Mohammed, Y. Cui, H. N. Alshareef, Concentrated dual-cation electrolyte strategy for aqueous zinc-ion batteries, Energy Environ. Sci. 14 (2021) 4463–4473, https://doi.org/10.1039/D1EE01472B.
[15] C. Li, S. Jin, L.A. Archer, L.F. Nazar, Toward practical aqueous zinc-ion batteries for electrochemical energy storage, Joule 6 (2022) 1733–1738, https://doi.org/10.1016/j.joule.2022.06.002.
[16] B. Qiu, K. Liang, W. Huang, G. Zhang, C. He, P. Zhang, H. Mi, Crystal-facet manipulation and interface regulation via TMP-modulated solid polymer electrolytes toward high-performance Zn metal batteries, Adv. Energy Mater. 13 (2023) 2301193, https://doi.org/10.1002/aenm.202301193.
[17] Y. Wang, Z. Wang, W.K. Pang, W. Lie, J.A. Yuwono, G. Liang, S. Liu, A.M. Angelo, J. Deng, Y. Fan, K. Davey, B. Li, Z. Guo, Solvent control of water O-H bonds for highly reversible zinc ion batteries, Nat. Commun. 14 (2023) 2720, https://doi.org/10.1038/s41467-023-38384-x.
[18] G. Ma, L. Miao, W. Yuan, K. Qiu, M. Liu, X. Nie, Y. Dong, N. Zhang, F. Cheng, Non-flammable, dilute, and hydrous organic electrolytes for reversible Zn batteries, Chem. Sci. 13 (2022) 11320–11329, https://doi.org/10.1039/D2SC04143J.
[19] J. Han, A. Mariani, M. Zarrabeitia, Z. Jusys, R.J. Behm, A. Varzi, S. Passerini, Zinc-ion hybrid supercapacitors employing acetate-based water-in-salt electrolytes, Small 18 (2022) e2201563, https://doi.org/10.1002/smll.202201563.
[20] M. Wu, W. Su, X. Wang, Z. Liu, F. Zhang, Z. Luo, A. Yang, P. Yeleken, Z. Miao, Y. Huang, Long-life aqueous zinc–organic batteries with a trimethyl phosphate electrolyte and organic cathode, ACS Sustain. Chem. Eng. 11 (2023) 957–964, https://doi.org/10.1021/acssuschemeng.2c05410.
[21] T. Zhang, J. Yang, H. Wang, H. Yu, Q. Li, L. Chen, Y. Chen, T. Wang, A solubility-limited, non-protonic polar small molecule co-solvent reveals additive selection in inorganic zinc salts, Energy Storage Mater. 65 (2024) 103085, https://doi.org/10.1016/j.ensm.2023.103085.
[22] H. Fei, F. Yang, Z. Jusys, S. Passerini, A. Varzi, Ethylene glycol co-solvent enables stable aqueous ammonium-ion batteries with diluted electrolyte, Adv. Funct. Mater. (2024) 2404560.

[23] Q. Li, C. Yang, J. Zhang, X. Ji, J. Xu, X. He, L. Chen, S. Hou, J. Uddin, D. Addison, D. Sun, C. Wang, F. Wang, Controlling intermolecular interaction and interphase chemistry enabled sustainable water-tolerance $LiMn_2O_4||Li_4Ti_5O_{12}$ batteries, Angew. Chem.-Int. Ed. 61 (2022) e202214126, https://doi.org/10.1002/anie.202214126.
[24] N. Tekin, M. Cebe, Solvents effect on infrared spectra of trimethyl phosphate in organic solvents, Vib. Spectrosc 36 (2004) 129–133, https://doi.org/10.1016/j.vibspec.2004.05.001.
[25] Z.H. Ping, Q.T. Nguyen, S.M. Chen, J.Q. Zhou, Y.D. Ding, States of water in different hydrophilic polymers — DSC and FTIR studies, Polymer 42 (2001) 8461–8467, https://doi.org/10.1016/S0032-3861(01)00358-5.
[26] Z. Tian, J. Yin, T. Guo, Z. Zhao, Y. Zhu, Y. Wang, J. Yin, Y. Zou, Y. Lei, J. Ming, O. Bakr, O.F. Mohammed, H.N. Alshareef, A sustainable NH4+ ion battery by electrolyte engineering, Angew. Chem. Int. Ed. Engl. 61 (2022) e202213757, https://doi.org/10.1002/anie.202213757.
[27] Y. Zhao, Z. Tian, W. Wang, X. Deng, J.-C. Tseng, G.-H. Wang, Size-dependent activity of Fe-N-doped mesoporous carbon nanoparticles towards oxygen reduction reaction, Green Carbon 2 (2024) 221–230, https://doi.org/10.1016/j.greenca.2024.03.002.
[28] K.-H. Kim, Y.-H. Kim, Theoretical studies for the supercritical CO_2 solubility of organophosphorous molecules: Lewis acid-base interactions and C-H···O weak hydrogen bonding, Bull. Kor. Chem. Soc. 28 (2007) 2454–2458, https://doi.org/10.5012/bkcs.2007.28.12.2454.
[29] R. Zhang, W.K. Pang, J. Vongsvivut, J. Yuwono, G. Li, Y. Lyu, Y. Fan, Y. Zhao, S. Zhang, J. Mao, Q. Cai, S. Liu, Z. Guo, Weakly solvating aqueous-based electrolyte facilitated by a soft co-solvent for extreme temperature operations of zinc-ion batteries, Energy Environ. Sci. 17 (2024) 4569–4581, https://doi.org/10.1039/d4ee00942h.
[30] J. Zhou, F. Wu, Y. Mei, W. Ma, L. Li, R. Chen, Highly stable aqueous/organic hybrid zinc-ion batteries based on a synergistic cathode/anode interface engineering, ACS Nano 18 (2024) 839–848, https://doi.org/10.1021/acsnano.3c09419.
[31] H. Liu, Y. Zhang, C. Wang, J.N. Glazer, Z. Shan, N. Liu, Understanding and controlling the nucleation and growth of Zn electrodeposits for aqueous zinc-ion batteries, ACS Appl. Mater. Interfaces 13 (2021) 32930–32936, https://doi.org/10.1021/acsami.1c06131.
[32] L. Ma, M.A. Schroeder, T.P. Pollard, O. Borodin, M.S. Ding, R. Sun, L. Cao, J. Ho, D. R. Baker, C. Wang, Critical factors dictating reversibility of the zinc metal anode, Energy Environ. Mater. 3 (2020) 516–521, https://doi.org/10.1002/eem2.12077.
[33] H. Fei, J. Han, S. Passerini, A. Varzi, Hybrid organic/inorganic interphase for stabilizing a zinc metal anode in a mild aqueous electrolyte, ACS Appl. Mater. Interfaces 14 (2022) 48675–48681, https://doi.org/10.1021/acsami.2c13645.
[34] P. Xiao, H. Li, J. Fu, C. Zeng, Y. Zhao, T. Zhai, H. Li, An anticorrosive zinc metal anode with ultra-long cycle life over one year, Energy Environ. Sci. 15 (2022) 1638–1646, https://doi.org/10.1039/D1EE03882F.
[35] C.D. Wagner, A. Joshi, The auger parameter, its utility and advantages: a review, J. Electron Spectrosc. Relat. Phenom. 47 (1988) 283–313, https://doi.org/10.1016/0368-2048(88)85018-7.
[36] L. Dake, D. Baer, J. Zachara, Auger parameter measurements of zinc compounds relevant to zinc transport in the environment, Surf. Interface Anal. 14 (1989) 71–75, https://doi.org/10.1002/sia.740140115.
[37] C. Lin, X. Yang, P. Xiong, H. Lin, L. He, Q. Yao, M. Wei, Q. Qian, Q. Chen, L. Zeng, High-rate, large capacity, and long life dendrite-free Zn metal anode enabled by trifunctional electrolyte additive with a wide temperature range, Adv. Sci. 9 (2022), https://doi.org/10.1002/advs.202201433.
[38] L. Caracciolo, L. Madec, H. Martinez, XPS analysis of K-based reference compounds to allow reliable studies of solid electrolyte interphase in K-ion batteries, ACS Appl. Energy Mater. 4 (2021) 11693–11699.
[39] J. Zhang, W. Huang, L. Li, C. Chang, K. Yang, L. Gao, X. Pu, Nonepitaxial electrodeposition of (002)-textured Zn anode on textureless substrates for dendrite-free and hydrogen evolution-suppressed Zn batteries, Adv. Mater. 35 (2023), https://doi.org/10.1002/adma.202300073.
[40] Z. Huang, Z. Li, Y. Wang, J. Cong, X. Wu, X. Song, Y. Ma, H. Xiang, Y. Huang, Regulating Zn(002) deposition toward long cycle life for Zn metal batteries, ACS Energy Lett. 8 (2022) 372–380, https://doi.org/10.1021/acsenergylett.2c02359.
[41] Y. Yang, S. Liang, B. Lu, J. Zhou, Eutectic electrolyte based on N-methylacetamide for highly reversible zinc–iodine battery, Energy Environ. Sci. 15 (2022) 1192–1200, https://doi.org/10.1039/d1ee03268b.
[42] L. Suo, O. Borodin, T. Gao, M. Olguin, J. Ho, X. Fan, C. Luo, C. Wang, K. Xu, "Water-in-salt" electrolyte enables high-voltage aqueous lithium-ion chemistries, Science 350 (2015) 938–943, https://doi.org/10.1126/science.aab1595.
[43] F. Yang, J. Long, J.A. Yuwono, H. Fei, Y. Fan, P. Li, J. Zou, J. Hao, S. Liu, G. Liang, Y. Lyu, X. Zheng, S. Zhao, K. Davey, Z. Guo, Single atom catalysts for triiodide adsorption and fast conversion to boost the performance of aqueous zinc–iodine batteries, Energy Environ. Sci. 16 (2023) 4630–4640, https://doi.org/10.1039/d3ee01453c.